Hindawi
Advances in Civil Engineering
Volume 2022, Article ID 3100011, 12 pages
https://doi.org/10.1155/2022/3100011

Research Article

Potential Roof Collapse Analysis of Tunnel Considering the Orthotropic Weak Interlayer on the Detaching Surface

Tong Xu,[1] **Dingli Zhang**,[1] **Zhenyu Sun**,[1] **Lin Yu**,[1] **Ran Li**,[2] **and Jiwei Luo**[3]

[1]*Key Laboratory of Urban Underground Engineering of Ministry of Education, Beijing Jiaotong University, Beijing 100044, China*
[2]*China Tiesiju Civil Engineering Group Co., Ltd., Hefei 230023, China*
[3]*Tianjin Research Institute for Water Transport Engineering, M.O.T, Tianjin 300456, China*

Correspondence should be addressed to Tong Xu; 16115280@bjtu.edu.cn

Received 11 July 2022; Accepted 4 August 2022; Published 27 September 2022

Academic Editor: Pengjiao Jia

The evaluation of the roof collapse in tunnels or cavities remains one of the most complex issues in geotechnical engineering. Taking the detaching surface of the tunnel roof collapse as an orthotropic weak interlayer, an analytical approach for determining the limit collapse range considering the arch effect of the tunnel is presented in this paper by the variation calculus. A discontinuity criterion moving from the anisotropic criterion proposed by the present authors is applied to the orthotropic interlayer. The phenomenon of sharp points in collapse blocks is further analyzed. Based on the proposed approach, illustrated examples are analyzed to investigate the effect of the strength parameters and the consideration of the collapse cusp, which show different influence laws on the range of collapse blocks. Those interesting conclusions can provide guidance for the prediction of the collapse mechanism of the tunnel.

1. Introduction

The stability problems of tunnels have always been of overriding significance in geotechnical engineering. The possible collapse of the tunnel remains one of the most challenging problems. Due to the natural uncertainties of the properties of the rock mass in situ, such as mechanical parameters and the random variability of cracks or fractures [1–8], the collapse mechanism of a cavity roof has yet to be thoroughly grasped [9]. Because the limit analysis method requires no elastic characterization and only refers to the limit behavior, this approach can obtain more rigorous results with fewer assumptions [10]. As a result, the limit analysis method is very suitable for analyzing the collapse mechanism of tunnel roofs and has been rapidly developed in recent years.

Lippmann [11] firstly applied the limit analysis method to the roof stability problems of tunnels considering the Mohr–Coulomb (M-C) criterion. For many years, the roof stability of tunnels is analyzed in this framework [10]. Guarracino and Guarracino [12] made encouraging progress with the help of plasticity theory and calculus of variations, and a closed-form solution of the collapsed outline was obtained with the Hoek–Brown (H-B) criterion considered instead of the M-C rule. Since then, many researchers furthered their work by considering various cases of cavities such as different excavation profiles [13], layered rock masses or soils [9, 14–17], the presence of the karst cave [18], the solutions for shallow tunnels [19–22] or progressive collapse [23–26], consideration of the supporting pressure [27–29], and the case considering the groundwater [30–33].

These extending works moving from the approaches of Guarracino and Guarracino [12] only focused on the H-B rule expressed in the M-C form (nonlinear). In fact, a weak interlayer may appear between the detaching surface when roof collapse occurs [34]. The rock mass at the detaching surface of the collapse zone can be taken as a weak interlayer with thin thickness, which is related to the failure mechanism of the surrounding rock [35, 36]. Under the influence of the dislocation of the rock masses, the weak interlayer exhibits different strength characteristics in the orthogonal direction. For this reason, analysis considering the

orthotropic characteristics of the weak interlayer between the detaching surface can better describe the roof collapse problems of tunnels or cavities. This consideration requires a special criterion that can describe the failure behavior of the orthotropic weak interlayer on the detaching surface.

In addition, we notice that most researchers obtained a smooth collapse curve, which can be derivable at the axis of symmetry [24]. In fact, a collapse cusp (not derivable at the axis of symmetry) is usually observed in model tests or numerical analysis [34, 37, 38], which means that the condition at the axis of symmetry should be treated with caution (Figure 1). To further explain this phenomenon, the sharp point of the collapse curve is discussed in our study. Once the assumption of a smooth curve (at the axis of symmetry) is not applied to the analysis, it becomes more difficult to get the collapse curve. As a result, we need to find a reasonable restriction as an alternative to the smooth assumption when considering the collapse cusp.

Based on the above considerations, a discontinuity yield criterion for an orthotropic interlayer that moves from a pressure-dependent, anisotropic criterion is applied in this research. Then, the theoretical formulas for the cases with and without considering the collapse cusp are deduced to figure up the collapse block. Finally, some examples are analyzed, and the discrepancy between different cases is further discussed in this paper. The results can help constitute guidance for the prediction of the collapse range of tunnels or cavities.

2. Problem Description

2.1. Orthotropic Criterion at the Velocity Discontinuity. The orthotropic yield criterion can move from the anisotropic criterion. Given the pressure-dependent of the rock material, Caddell et al. [39] proposed an anisotropic yield criterion in the following form:

$$\begin{aligned} &A_{yz}\left(\sigma_y-\sigma_z\right)^2+A_{zx}\left(\sigma_z-\sigma_x\right)^2+A_{xy}\left(\sigma_x-\sigma_y\right)^2\\ &+B_{yz}\tau_{yz}^2+B_{zx}\tau_{zx}^2+B_{xy}\tau_{xy}^2+K_1\sigma_x+K_2\sigma_y+K_3\sigma_z=1, \end{aligned} \tag{1}$$

where the parameters A_{yz}, A_{zx}, A_{xy}, B_{yz}, B_{zx}, B_{xy}, K_1, K_2, and K_3 characterize the properties of anisotropy. The subscript x, y, and z denote the reference axes of anisotropy. In consideration of the orthotropic materials, these parameters satisfy the following relations:

$$A_{yz}=A_{zx}, B_{yz}=B_{zx}, B_{xy}=2\left(A_{yz}+2A_{xy}\right), K_1=K_2. \tag{2}$$

Because the detaching surface is consistent with the weak layer, we take the normal direction of the detaching surface as the z axis (Figure 2). As a result, the failure on the detaching surface only depends on σ_z, τ_{zy}, and τ_{zx}, which leads to an orthotropic yield criterion in the degenerative form:

$$B_{zx}\left(\tau_{zx}^2+\tau_{zy}^2\right)+K_3\sigma_z=1. \tag{3}$$

For the plane strain problems, the equation (3) can be further simplified as

$$B\tau^2+K\sigma_n=1, \tag{4}$$

where σ_n denotes the stress of normal direction (the compressive stress is taken as positive in this paper), and the parameters B and K can be determined according to the shear (τ_0) and tensile (σ_T) strengths of the weak interlayer on the detaching surface.

$$B=\frac{1}{\tau_0^2}, K=-\frac{1}{\sigma_T}. \tag{5}$$

On the basis of the above consideration, the discontinuity yield criterion at the detaching surface of velocity can be obtained as

$$f=\tau^2-\tau_0^2\sigma_T^{-1}\sigma_n-\tau_0^2=0. \tag{6}$$

2.2. Collapse Mechanism of the Tunnel Roof. The key point about the roof stability of tunnels or cavities is to determine the shape and range of the potential collapsing blocks (Figure 3). As it is usual, this paper considers the problem in a plane and only makes reference to the cross section of a long tunnel or cavity. The rock material is assumed to be ideally plastic, and the plastic strain rate follows the associated flow rule. Besides, strain within the collapsing body is regarded as insignificant when the roof collapse occurs (rigid-plastic behavior). Based on the above conditions, the shape of the potential collapsing region can be given by using the calculus of variations [12, 40].

In order to investigate the roof collapse on account of the gravity field and refer to the upper bound principle [41], a kinematically admissible field of vertical velocity, which fulfills the compatibility with the strain rates, must be assumed at first [42]. As shown in Figure 3, the collapse velocity $\dot{u}_v$ is in the negative direction of the y-axis, and the symmetrical collapse curve is expressed as $f(x)$. Moreover, as shown in Figure 4, the value of the vertical velocity is considered a variable that decreases from $\dot{u}$ ($x=0$) to zero ($x=R$) linearly. As a result, the field of the variable vertical velocity can be expressed as

$$\dot{u}_v=\dot{u}\left(1-\frac{x}{R}\right). \tag{7}$$

According to the geometric conditions, the plastic strain rate (the tensile strain rate is taken as negative) components in the tangential ($\dot{\gamma}$) and normal ($\dot{\varepsilon}_n$) directions can be obtained as

$$\begin{aligned} \dot{\gamma}&=-\left(1-\frac{x}{R}\right)\left(\frac{\dot{u}}{w}\right)f'(x)\left[1+f'(x)^2\right]^{-\frac{1}{2}},\\ \dot{\varepsilon}_n&=-\left(1-\frac{x}{R}\right)(\dot{u}/w)\left[1+f'(x)^2\right]^{-\frac{1}{2}}. \end{aligned} \tag{8}$$

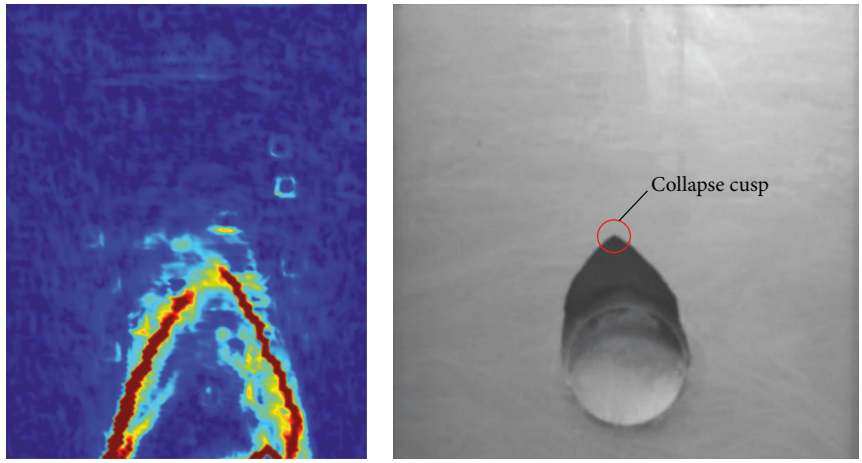

(a) (b)

Figure 1: Roof collapse in (a) an active trapdoor numerical test [34]; (b) a model test [38].

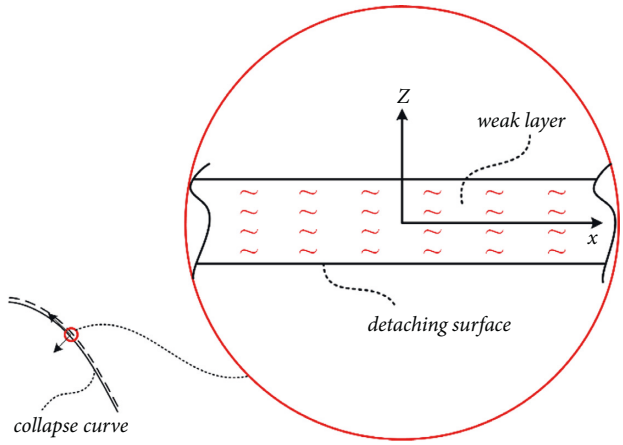

Figure 2: Orthotropic interlayer on the detaching surface.

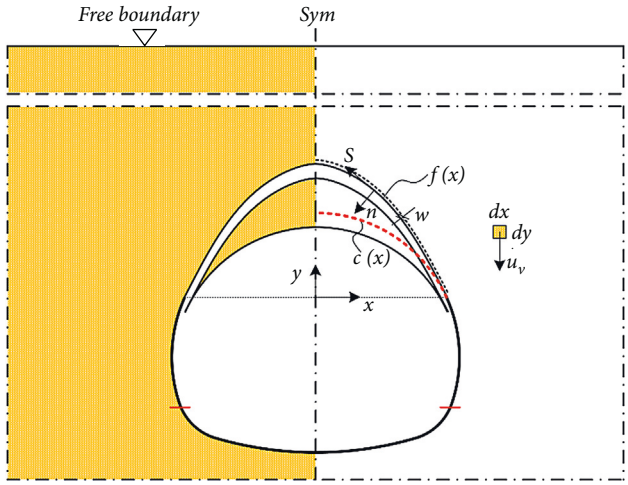

Figure 3: Possible collapsing area of the tunnel roof.

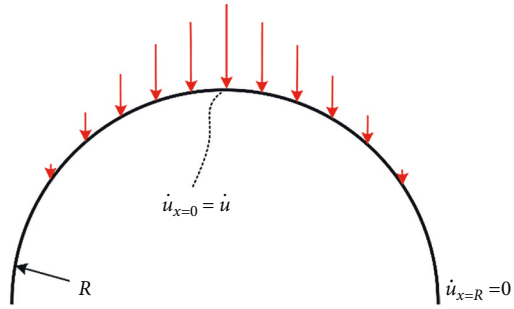

Figure 4: The field of the variable vertical velocity.

Coincident with the failure criterion mentioned in Section 2.1 (obeying to the associated flow rule), the plastic potential function ξ can be expressed as

$$\xi = \tau^2 - \tau_0^2 \sigma_T^{-1} \sigma_n - \tau_0^2. \tag{9}$$

Further, the plastic strain rate can also be written in the form:

$$\dot{\gamma} = \lambda \frac{\partial \xi}{\partial \tau} = 2\lambda\tau,$$
$$\dot{\varepsilon}_n = \lambda \frac{\partial \xi}{\partial \sigma_n} = -\lambda \tau_0^2 \sigma_T^{-1}. \tag{10}$$

The association of equations (7) and (9) leads to the following results:

$$\lambda = \tau_0^{-2} \sigma_T \left(1 - \frac{x}{R}\right)\left(\frac{\dot{u}}{w}\right)\left[1 + f'(x)^2\right]^{-\frac{1}{2}} \tag{11}$$

$$\tau = -\frac{\tau_0^2 \sigma_T^{-1}}{2} f'(x). \tag{12}$$

Finally, by substituting equations (10) into (6), we can obtain

$$\sigma_n = \frac{\tau_0^2 \sigma_T^{-1}}{4} f'(x)^2 - \sigma_T. \tag{13}$$

According to the equations (11) and (12), the tangential and normal stress components are expressed by using the derivative of the collapse function. Because a cusp (Figure 1) can occur in roof collapse [34, 37, 38], the stress at the axis of symmetry should be treated with caution (no derivative). In particular, the shear stresses around the collapse cusp can be described in Figure 5. Based on symmetry, the magnitude of the shear stresses in the symmetrical tilt directions at the cusp point must be equal. As a result, the inner horizontal shear stress at the axis of symmetry naturally satisfies the condition of being equal to zero, so long as the collapse curves on both sides are symmetrical to each other.

3. Analysis without Considering Collapse Cusp

Because most researchers assumed a smooth collapse curve in their studies [23, 24], the collapse curve is derivable at the axis of symmetry, which must lead to zero of derivative

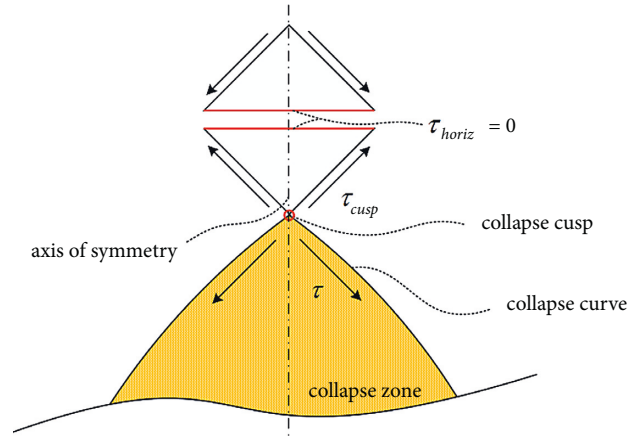

Figure 5: The shear stresses around the collapse cusp.

function $f'(x)$. For comparison, we analyze the collapse curve without considering collapse cusp in this section. Meanwhile, a different criterion (i.e., the orthotropic yield criterion proposed in section 2.1) is applied at the velocity discontinuity.

Associating the equations (7), (11), and (12), the dissipated power density of the internal stresses at the discontinuity ($\dot{D}$) is expressed as

$$\dot{D} = \sigma_n \dot{\varepsilon}_n + \tau\dot{\gamma}$$
$$= \left\{\left(\frac{\tau_0^2 \sigma_T^{-1}}{4} f'(x)^2 + k\sigma_T\right) \Big/ \left(w\sqrt{1 + \left[f'(x)\right]^2}\right)\right\}\left(1 - \frac{x}{R}\right)\dot{u}. \tag{14}$$

Besides, the power density of the applied loads is

$$\dot{W}_e = \gamma\left[f(x) - c(x)\right]\left(1 - \frac{x}{R}\right)\dot{u}, \tag{15}$$

where γ denotes the gravity per unit volume of the rock mass.

Here, we consider the right half of the symmetrical block (with respect to the y-axis). The total dissipated power of the collapse system is further deduced as

$$\dot{U} = \int_0^L \dot{D} w \sqrt{1 + \left[f'(x)\right]^2} dx - \int_0^L \dot{W}_e dx$$
$$= \int_0^L F\left[f(x), f'(x), x\right] \dot{u} dx, \tag{16}$$

where the $F[f(x), f'(x), x]$ can be expressed as

$$F\left[f(x), f'(x), x\right] =$$
$$\left\{\frac{\tau_0^2 \sigma_T^{-1}}{4} f'(x)^2 + \sigma_T - \gamma\left[f(x) - c(x)\right]\right\}\left(1 - \frac{x}{R}\right)\dot{u}. \tag{17}$$

Because the effective collapse curve can be obtained when the total dissipation power makes a minimum [13], the problem can be solved by using the calculus of variations. In order to obtain an extremum of the total dissipated power $\dot{U}$ over the interval of 0-L, the functional F must satisfy Euler's equation:

$$\delta\dot{U} = 0 \Rightarrow \frac{\partial F}{\partial f(x)} - \frac{d}{dx}\left(\frac{\partial F}{\partial f'(x)}\right) = 0. \tag{18}$$

From equation (14), we can deduce that

$$\frac{\partial F}{\partial f(x)} = -\gamma\left(1 - \frac{x}{R}\right)\dot{u}, \frac{\partial F}{\partial f'(x)}$$

$$= \frac{1}{2}\tau_0^2\sigma_T^{-1} f'(x)\left(1 - \frac{x}{R}\right)\dot{u}, \tag{19}$$

$$\frac{d}{dx}\left(\frac{\partial F}{\partial f'(x)}\right) = \frac{1}{2}\tau_0^2\sigma_T^{-1}\left[f''(x)\left(1 - \frac{x}{R}\right) - \frac{1}{R}f'(x)\right]\dot{u}.$$

By substituting equations (16) into (15), it is

$$\left\{-\gamma\left(1 - \frac{x}{R}\right) - \frac{1}{2}\tau_0^2\sigma_T^{-1}\left[f''(x)\left(1 - \frac{x}{R}\right) - \frac{1}{R}f'(x)\right]\right\}\dot{u} = 0. \tag{20}$$

Integrating the equation (17), we can obtain the first derivative of $f(x)$ as follows:

$$f'(x) = \gamma\tau_0^{-2}\sigma_T\left(R - x - \frac{R^2}{R - x}\right) + \frac{C_1 R}{R - x}. \tag{21}$$

Here, C_1 is an unknown parameter which needs to be further determined. Similar to existing studies, $f'(x = 0)$ should be equal to zero because a smooth symmetrical collapse curve is assumed in this section, which results in $C_1 = 0$. Then, the collapse curve $f(x)$ can be deduced by integrating the equation (18):

$$f(x) = \gamma\tau_0^{-2}\sigma_T\left(Rx - \frac{1}{2}x^2 + R^2\ln(R - x)\right) + C_2, \tag{22}$$

where C_2 is a pending parameter. Considering an implicit constraint $f(x = L) = 0$, we can obtain that

$$C_2 = -\gamma\tau_0^{-2}\sigma_T\left(RL - \frac{1}{2}L^2 + R^2\ln(R - L)\right), \tag{23}$$

$$c(x) = \sqrt{R^2 - x^2} - \sqrt{R^2 - L^2}. \tag{24}$$

Then, L can be further determined by equating the total dissipated power to zero. Substituting equations (15) and (20)–(23) into (14), we can obtain the equation which L yields. It is

$$\frac{\gamma^2\sigma_T R^3}{4\tau_0^2}\left\{\frac{L}{R} + \frac{1}{2}\left(\frac{L}{R}\right)^2 - \left(\frac{L}{R}\right)^3 + \frac{1}{4}\left(\frac{L}{R}\right)^4 - \ln\left(\frac{R}{R - L}\right)\right\}$$

$$-\gamma\left\{\frac{R^2}{3} - \frac{R^2}{2}\arcsin\left(\frac{L}{R}\right) + \frac{R}{6}\left[\frac{3L}{R} - \left(\frac{L}{R}\right)^2 - 2\right]\left(R^2 - L^2\right)^{\frac{1}{2}}\right\}$$

$$+\frac{\sigma_T L}{2}\left(2 - \frac{L}{R}\right) = 0 \tag{25}$$

Note that equation (23) can be easily solved by using the numerical method. After L is obtained, the collapse curve is finally written as

$$f(x) = \begin{cases} \gamma\tau_0^{-2}\sigma_T\left(R(x - L) + \frac{1}{2}\left(L^2 - x^2\right) + R^2\ln\left(\frac{R - x}{R - L}\right)\right), (x \geq 0) \\ \gamma\tau_0^{-2}\sigma_T\left(R(-x - L) + \frac{1}{2}\left(L^2 - x^2\right) + R^2\ln\left(\frac{R + x}{R - L}\right)\right), (x < 0) \end{cases}. \tag{26}$$

4. Analysis Considering Collapse Cusp

When a possible collapse cusp (Figure 5) is considered in the collapse analysis, the condition at the axis of symmetry should be handled with care due to no derivative. As a result, C_1 in equation (19) cannot be simply determined by equating $f'(x = 0)$ with zero. So, $f(x)$ coming from equation (18) should be written as

$$f(x) = \gamma\tau_0^{-2}\sigma_T\left(Rx - \frac{1}{2}x^2 + R^2\ln(R - x)\right) - C_1 R\ln(R - x) + C_2. \tag{27}$$

Then, the pending parameter C_2 can be deduced by considering $f(x = L) = 0$. It results

$$C_2 = -\gamma\tau_0^{-2}\sigma_T\left(RL - \frac{1}{2}L^2 + R^2\ln(R - L)\right) + C_1 R\ln(R - L). \tag{28}$$

Substituting equations (17), (24), (27), and (28) into (14) and equating the total dissipated power to zero, C_1 and L yield

$$\frac{\gamma^2\sigma_T R^3}{4\tau_0^2}\left\{\frac{L}{R} + \frac{1}{2}\left(\frac{L}{R}\right)^2 - \left(\frac{L}{R}\right)^3 + \frac{1}{4}\left(\frac{L}{R}\right)^4 - \ln\left(\frac{R}{R - L}\right)\right\}$$

$$-\frac{\gamma R^2}{6}\left\{\begin{array}{c} 2 - 3\arcsin\left(\frac{L}{R}\right) \\ \\ +\left[\frac{3L}{R} - \left(\frac{L}{R}\right)^2 - 2\right]\left(1 - \left(\frac{L}{R}\right)^2\right)^{\frac{1}{2}} \end{array}\right\} \tag{29}$$

$$+\frac{\sigma_T L}{2}\left(2 - \frac{L}{R}\right) + \frac{C_1^2\tau_0^2 R}{4\sigma_T}\ln\left(\frac{R}{R - L}\right) = 0.$$

In addition, the fracturing azimuth is related to the friction angle (φ) of the surrounding rock. Taking a stress element at the collapse cusp of the tunnel and considering the friction angle (Figure 6), we can get the angle between directions of the fracture and maximum principal stress (the horizontal and vertical shear stresses, i.e., τ_{horiz} and τ_{verti}, are zero at the axis of symmetry) as $(\pi/4 - \varphi/2)$. Then, the one-sided derivative $f'_+(x)$ can be expressed as

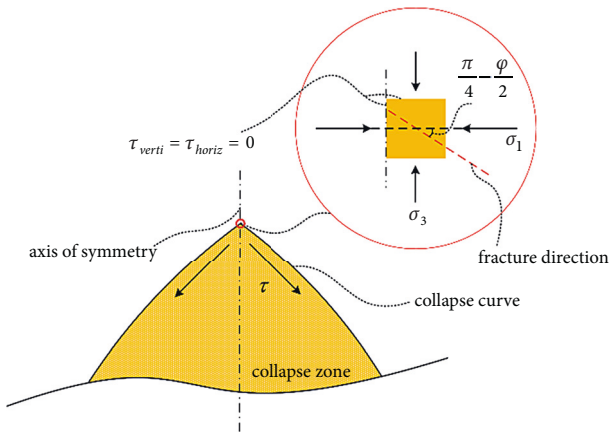

FIGURE 6: Microdescription of the fracture direction at the collapse cusp.

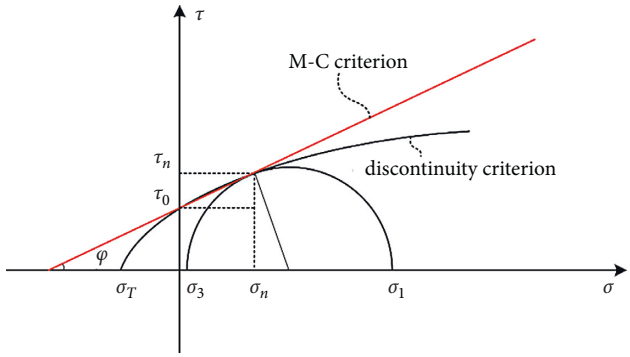

FIGURE 7: Acquisition of the friction angle by applying the M-C criterion.

$$f'_+(x=0) = C_1 = -\tan\left(\frac{\pi}{4}-\frac{\varphi}{2}\right). \tag{30}$$

The friction angle corresponding to the M-C criterion at the collapse cusp can be described in Figure 7. Considering

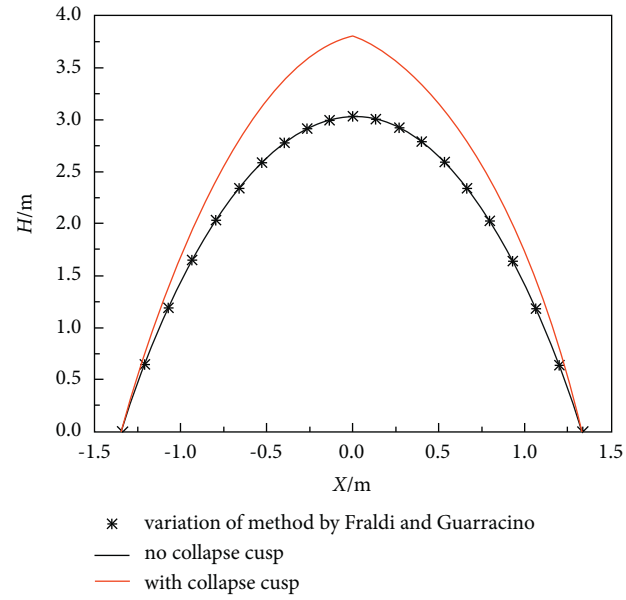

FIGURE 8: Comparison between cases considering and not considering the collapse cusp.

equation (30) and the approximate geometric conditions of σ_n and τ, the friction angle φ yields

$$\tan\varphi\tan^2\left(\frac{\pi}{4}-\frac{\varphi}{2}\right) - 2\tan\left(\frac{\pi}{4}-\frac{\varphi}{2}\right) + 4\tau_0^2\sigma_T(\tau_0 - \sigma_T\tan\varphi) = 0. \tag{31}$$

Finally, by considering equations (29), (30), and (31) together, we can get C_1 and L numerically. Then, the collapse curve considering a collapse cusp at the axis of symmetry ($x=0$) can be written as

$$f(x) = \begin{cases} \gamma\tau_0^{-2}\sigma_T\left(R(x-L) + \frac{1}{2}\left(L^2-x^2\right) + R^2\ln\left(\frac{R-x}{R-L}\right)\right) - C_1R\ln\left(\frac{R-x}{R-L}\right), & (x\geq 0) \\ \gamma\tau_0^{-2}\sigma_T\left(R(-x-L) + \frac{1}{2}\left(L^2-x^2\right) + R^2\ln\left(\frac{R+x}{R-L}\right)\right) - C_1R\ln\left(\frac{R+x}{R-L}\right), & (x<0) \end{cases}. \tag{32}$$

5. Examples and Discussion

5.1. The Discrepancy between Different Cases. In the preceding sections, two different analytical results are obtained by considering and not considering the collapse cusp, respectively. The two results obtained under different conditions are compared through an example. The parameters involved in the example are $\tau_0 = 20$ kPa, $\sigma_T = 22$ kPa, $\gamma = 25$ kN/m^3, and $R = 3$ m. As a result, the comparison between these two analytical results of the collapse curve is shown in Figure 8.

The results indicate that the collapse curve obtained by considering the collapse cusp is higher than that obtained without considering the collapse cusp. According to the analytical results obtained in this paper, the height of the collapse block can increase by 0.78 m when considering the collapse cusp in the analysis. The span of the collapse curve does not change whether the cusp is considered or not. Due to the increase in the collapse height, the weight of the collapse block will also increase. The gravity of the collapse block can be calculated by using the following equation:

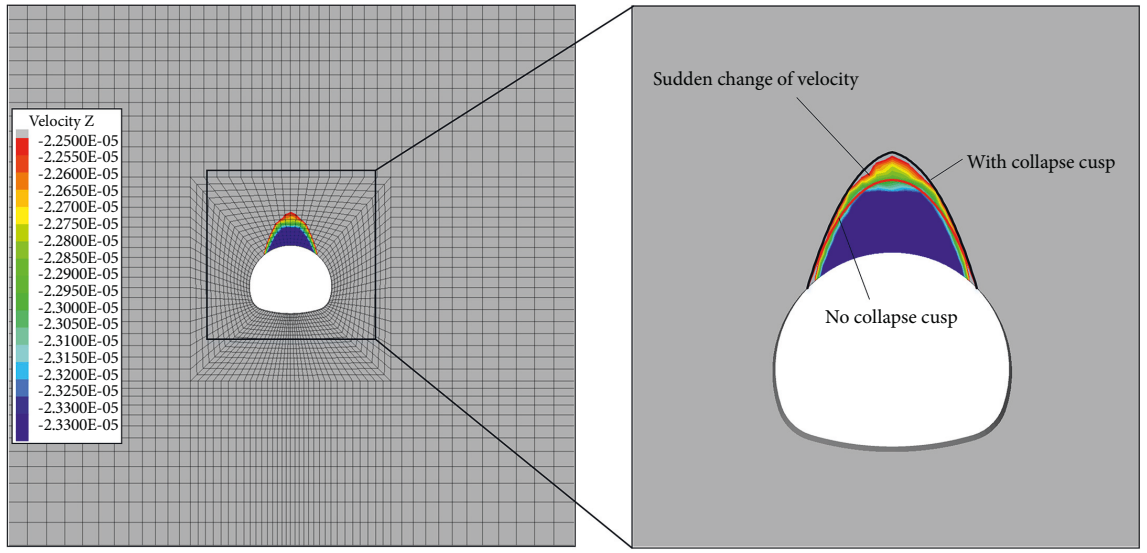

Figure 9: Comparison of collapse block shapes in terms of vertical velocities.

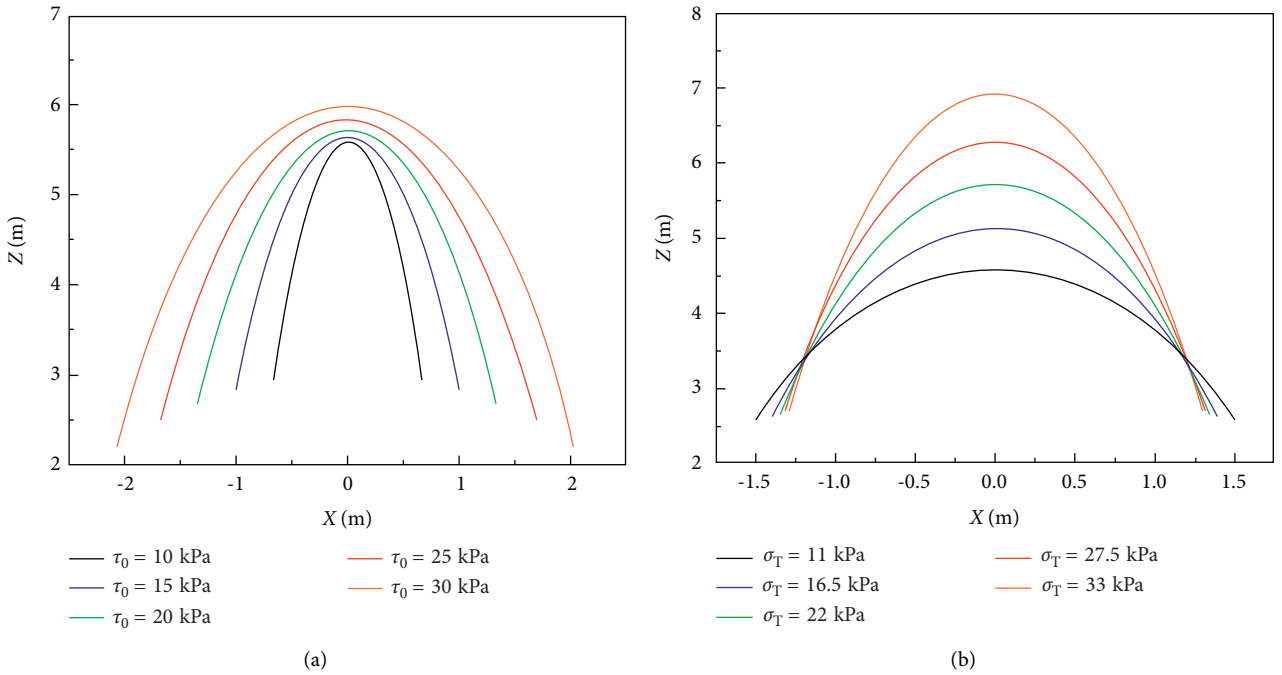

Figure 10: Effects of strength parameters involved in our analysis on the potential collapse of the tunnel roof without considering the collapse cusp: (a) shear strength; (b) tensile strength.

$$P = 2\int_0^L \gamma[f(x) - c(x)]dx. \tag{33}$$

Substituting equations (24) and (30) into (31), respectively, we can easily calculate the gravity corresponding to the collapse block for both cases. The results show that the gravity obtained by considering the collapse cusp is increased by 23% compared to the gravity obtained without considering the collapse cusp. Therefore, taking the collapse cusp at the axis of symmetry into account when predicting the collapse block can help ensure the safety of the tunnel roof.

5.2. Comparison with Numerical Analysis. A numerical analysis has been performed to further verify the above analyses. The numerical parameters are consistent with those mentioned in Section 5.1. The M-C friction angle can be calculated from equation (29). The results for the example in terms of vertical velocities have been obtained by FLAC3D. The collapse block described the sudden change of vertical velocities as shown in Figure 9.

By comparing the collapse block shapes as shown in Figure 9, it is worth highlighting the similarity of the collapse block shape from numerical analysis to that obtained by the proposed analytical method. Both analytical results can

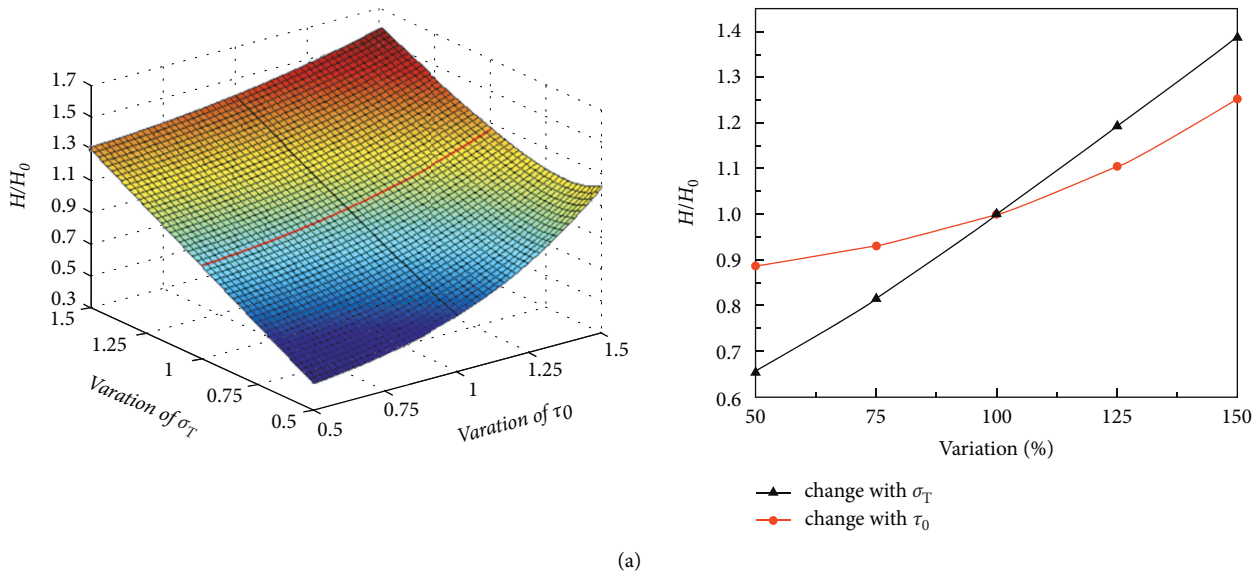

(a)

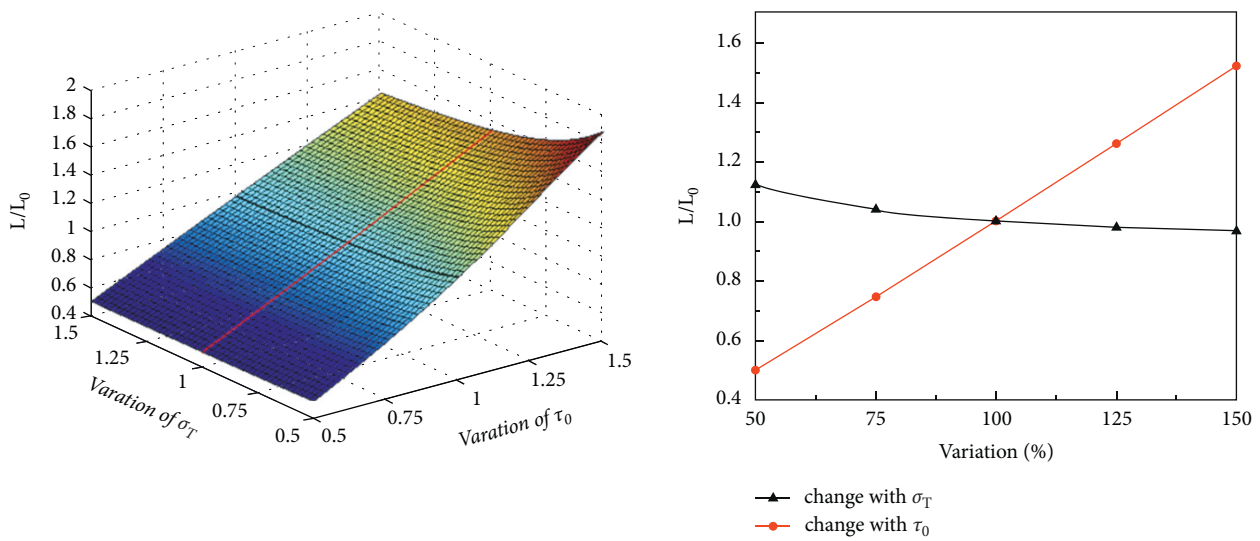

(b)

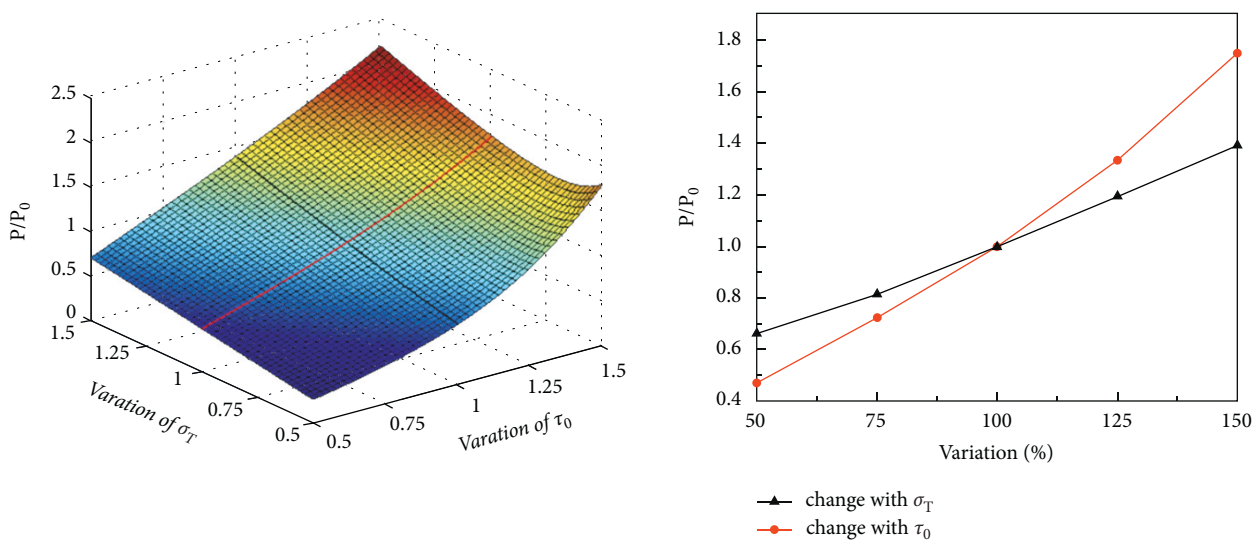

(c)

Figure 11: Comparison of the influences of shear and tensile strengths on (a) H/H_0; (b) L/L_0; (c) P/P.

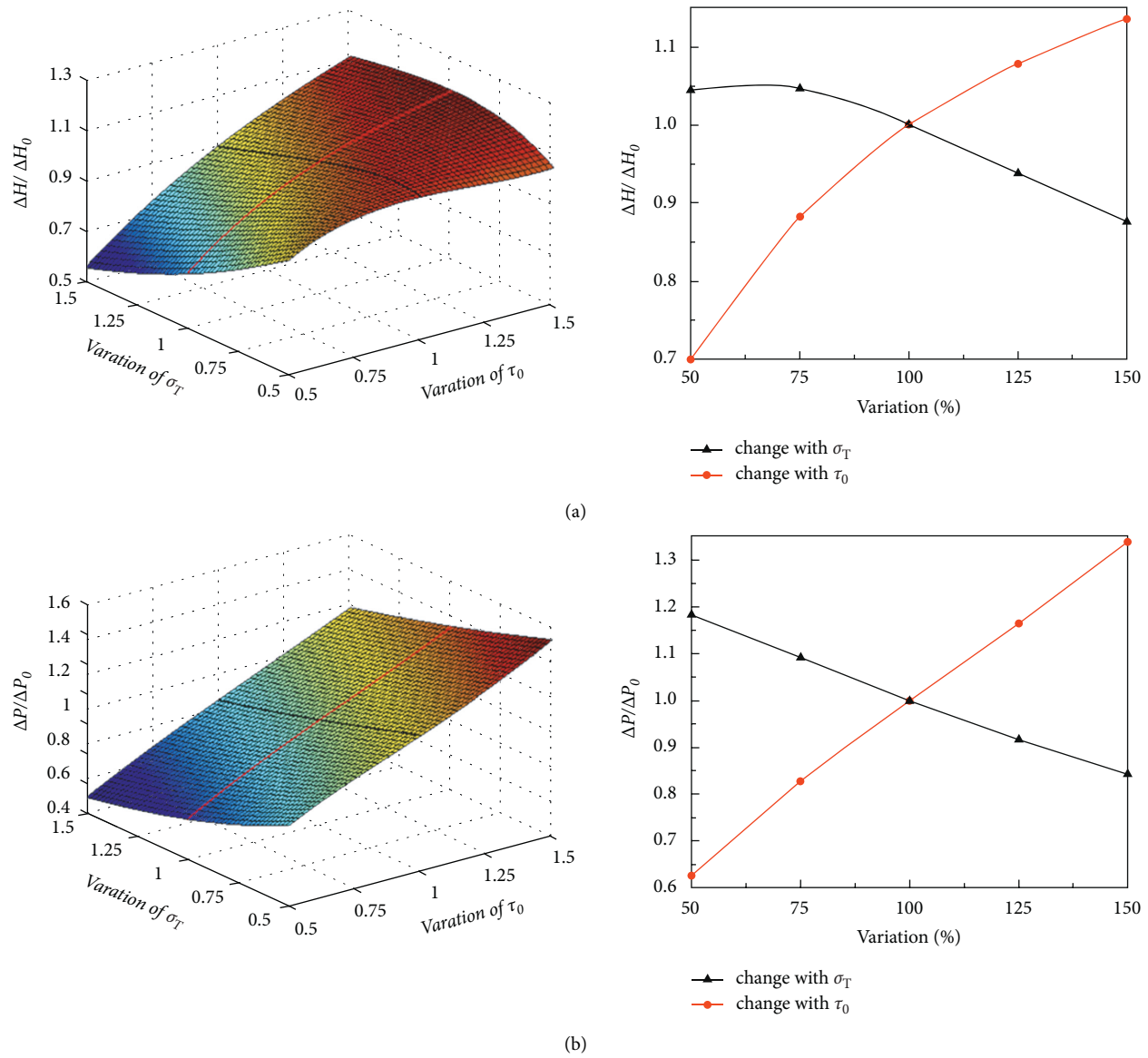

Figure 12: Comparison of the influences of shear and tensile strengths on the discrepancy between considering and not considering collapse cusp: (a) $\Delta H/\Delta H_0$; (b) $\Delta P/\Delta P_0$.

describe the collapse block shape well. As described in Section 5.1, the analytical result will lead to a wider range of collapse blocks when considering the phenomenon of sharp points in roof collapse behavior.

5.3. Influence of Strength Parameters of the Weak Interlayer. In the process of predicting the potential collapse of the tunnel roof, the shear and tensile strengths of the weak interlayer on the detaching surface are involved in our analysis. In order to investigate the influence of these two important parameters, we first discuss the different cases without considering the collapse cusp. Figures 10(a) and 10(b) show the different results considering different values of the shear and tensile strengths, respectively.

Figure 10(a) shows that the collapse curves obtained from our proposed analytical result are significantly affected by the shear strength of the weak interlayer on the detaching surface. The width and the height of the collapse block increase as the shear strength increases. Obviously, with the increase in shear strength, a greater gravity of surrounding rock can be maintained in the short term, but it also means that once the collapse occurs, there will be a wider range of primary failures.

Figure 10(b) shows that the collapse curves obtained from our proposed analytical result are also significantly affected by the tensile strength of the weak interlayer on the detaching surface. The height of the collapse block increases as the tensile strength increases. However, the width of the collapse block decreases as the tensile strength increases, which is different from the effect of the shear strength. Similar to the influence of shear strength, although the increase in tensile strength may maintain a greater gravity of surrounding rocks, there will be a wider range of primary failure once the collapse occurs.

Furthermore, in order to compare the different effects of shear and tensile strengths on the collapse block, the changes in height, width, and gravity of the collapse block are shown in Figures 11(a), 11(b), and 11(c), respectively. The example described in Section 5.1 is taken as the original case. By comparing the change rates of each index with different strength parameters, we can find that the height of the collapse block is more sensitive to the change in tensile strength. However, the width and the gravity of the collapse block are more sensitive to the change in shear strength.

As described in Section 5.1, the height and weight of the collapse block increase when considering the collapse cusp compared to those without considering the collapse cusp, while the span of the collapse curve does not change whether the cusp is considered or not. As a result, when considering the collapse cusp, only the changes in the collapse block height (ΔH) and gravity (ΔP) relative to the results without considering the collapse cusp are discussed. Figure 12 shows the comparison of the influences of shear and tensile strengths on the discrepancies of the collapse block height and gravity.

According to Figure 12, the discrepancies in the collapse block height and gravity between the two cases generally decrease with the increase in the tensile strength. On the contrary, the discrepancies in the collapse block height and gravity between the two cases increase with the increase in the shear strength. It is worth noting that these changes are more sensitive to the change of shear strength than the change of tensile strength, which is of directive functions when considering the effect of the consideration of the collapse cusp.

6. Conclusions

By using the orthotropic yield criterion which moves from the anisotropic criterion proposed by Caddell et al. [39] for the rock material, an exact solution to tunnel roof collapse has been obtained with the help of the traditional plasticity theory and the calculus of variations. In order to further illustrate the impact of collapse cusps which have been observed in previous studies [34, 37, 38], two different cases according to whether the collapse cusp is considered are analyzed in this paper. Our new theoretical results lead to the following conclusions:

(1) Taking the detaching surface of the tunnel roof collapse as an orthotropic weak interlayer, the theoretical formulas figuring up the collapse block are obtained with and without considering the collapse cusp, respectively. A case analysis shows that considering the collapse cusp can lead to a higher range of collapse blocks.

(2) The strength parameters of the weak interlayer have a significant impact on the range of collapse blocks. The shear and tensile strength have similar effects on the height of the collapse block, but their effects on the width have the opposite trend. Moreover, because the increase in shear and tensile strengths may maintain a greater gravity of surrounding rocks, there will be a wider range of primary failures once the collapse occurs. By sensitivity analysis, we can find that the height of the collapse block is more sensitive to the change in tensile strength, but the width and the gravity of the collapse block are more sensitive to the change of shear strength.

(3) The discrepancies between the two cases according to whether the collapse cusp considered are related to the strength parameters. The discrepancies between the two cases generally decrease with the increase in the tensile strength but increase with the increase in the shear strength. These changes are more sensitive to the change of shear strength than the change of tensile strength, which is of directive functions when considering the effect of the consideration of the collapse cusp.

Our theoretical results can provide guidance on the collapse mechanism in tunnels or natural cavities, especially they can explain the phenomenon of sharp points in collapse blocks. Moreover, based on our proposed approach, many extensions including various cases such as layered rock masses and the presence of the karst cave can be further studied in future research.

Data Availability

All data used to support the findings of this study are included within the article.

Conflicts of Interest

The authors declare that there are no conflicts of interest regarding the publication of this paper.

Acknowledgments

The authors gratefully acknowledge the National Natural Science Foundation of China (Grant no. 51738002).

References

[1] Z. Chu, Z. Wu, Q. Liu, B. Liu, and J. Sun, "Analytical solution for lined circular tunnels in deep viscoelastic burgers rock considering the longitudinal discontinuous excavation and sequential installation of liners," *Journal of Engineering Mechanics*, vol. 147, no. 4, 2021.

[2] Z. Chu, Z. Wu, Q. Liu, L. Weng, Z. Wang, and Y. Zhou, "Evaluating the microstructure evolution behaviors of saturated sandstone using NMR testing under uniaxial short-term and creep compression," *Rock Mechanics and Rock Engineering*, vol. 54, no. 9, pp. 4905–4927, 2021.

[3] Z. Chu, Z. Wu, Z. Wang, L. Weng, Q. Liu, and L. Fan, "Micromechanism of brittle creep in saturated sandstone and its mechanical behavior after creep damage," *International Journal of Rock Mechanics and Mining Sciences*, vol. 149, no. 3–4, p. 104994, 2022.

[4] Z. Sun, D. Zhang, Q. Fang, G. Dui, and Z. Chu, "Analytical solutions for deep tunnels in strain-softening rocks modeled by different elastic strain definitions with the unified strength theory," *Science China Technological Sciences*, vol. 65, 2022.

[5] Z. Sun, D. Zhang, Q. Fang, G. Dui, Q. Tai, and F. Sun, "Analysis of the interaction between tunnel support and surrounding rock considering pre-reinforcement," *Tunnelling and Underground Space Technology*, vol. 115, Article ID 104074, 2021.

[6] Z. Sun, D. Zhang, Q. Fang, D. Liu, and G. Dui, "Displacement process analysis of deep tunnels with grouted rockbolts considering bolt installation time and bolt length," *Computers and Geotechnics*, vol. 140, p. 104437, 2021.

[7] K. Wu, Z. Shao, M. Sharifzadeh, S. Hong, and S. Qin, "Analytical computation of support characteristic curve for circumferential yielding lining in tunnel design," *Journal of Rock Mechanics and Geotechnical Engineering*, vol. 14, no. 1, pp. 144–152, 2022.

[8] D. Zhang, Z. Sun, and Q. Fang, "Scientific problems and research proposals for Sichuan-Tibet railway tunnel construction," *Underground Space*, vol. 7, no. 3, pp. 419–439, 2022.

[9] C. Chian and S. C. Chian, "Revisiting crown stability of tunnels deeply buried in non-uniform rock surrounds," *Tunnelling and Underground Space Technology*, vol. 73, no. December, pp. 154–161, 2018.

[10] M. Fraldi, R. Cavuoto, A. Cutolo, and F. Guarracino, "Stability of tunnels according to depth and variability of rock mass parameters," *International Journal of Rock Mechanics and Mining Sciences*, vol. 119, no. May, pp. 222–229, 2019.

[11] H. Lippmann, "Plasticity in rock mechanics," *International Journal of Mechanical Sciences*, vol. 13, no. 4, pp. 291–297, July 1970.

[12] M. Guarracino and F. Guarracino, "Limit analysis of collapse mechanisms in cavities and tunnels according to the Hoek-Brown failure criterion," *International Journal of Rock Mechanics and Mining Sciences*, vol. 46, no. 4, pp. 665–673, 2009.

[13] M. Guarracino and F. Guarracino, "Analytical solutions for collapse mechanisms in tunnels with arbitrary cross sections," *International Journal of Solids and Structures*, vol. 47, no. 2, pp. 216–223, 2010.

[14] C. Chian and S. C. Chian, "2D and 3D stability analysis of tunnel roof collapse in stratified rock: a kinematic approach," *International Journal of Rock Mechanics and Mining Sciences*, vol. 100, no. October, pp. 269–277, 2017.

[15] X. L. Yang, T. Zhou, and W. T. Li, "Reliability analysis of tunnel roof in layered Hoek-Brown rock masses," *Computers and Geotechnics*, vol. 104, no. June, pp. 302–309, 2018.

[16] X. L. Yang and C. Yao, "Axisymmetric failure mechanism of a deep cavity in layered soils subjected to pore pressure," *International Journal of Geomechanics*, vol. 17, no. 8, Article ID 04017031, 2017.

[17] X. L. Yang and C. Yao, "Stability of tunnel roof in nonhomogeneous soils," *International Journal of Geomechanics*, vol. 18, no. 3, Article ID 06018002, 2018.

[18] C. Lyu, L. Yu, M. Wang, P. Xia, and Y. Sun, "Upper bound analysis of collapse failure of deep tunnel under karst cave considering seismic force," *Soil Dynamics and Earthquake Engineering*, vol. 132, p. 106003, 2020.

[19] C. Zeng and Z. Zeng, "Upper bound limit analysis of unsymmetrical progressive collapse of shallow tunnels in inclined rock stratum," *Computers and Geotechnics*, vol. 116, no. May, Article ID 103199, 2019.

[20] H. T. Wang, P. Liu, C. Liu, X. Zhang, Y. Yang, and L. Y. Liu, "Three-Dimensional upper bound limit analysis on the collapse of shallow soil tunnels considering roof stratification and pore water pressure," *Mathematical Problems in Engineering*, vol. 2019, pp. 1–15, 2019.

[21] X. L. Huang and F. Huang, "Collapse mechanism of shallow tunnel based on nonlinear Hoek-Brown failure criterion," *Tunnelling and Underground Space Technology*, vol. 26, no. 6, pp. 686–691, 2011.

[22] L. h. Zhao, S. h. Hu, X. P. Yang, F. Huang, and S. Zuo, "Limit variation analysis of shallow rectangular tunnels collapsing with double-layer rock mass based on a three-dimensional failure mechanism," *Journal of Central South University*, vol. 26, no. 7, pp. 1794–1806, 2019.

[23] M. Guarracino and F. Guarracino, "Limit analysis of progressive tunnel failure of tunnels in Hoek-Brown rock masses," *International Journal of Rock Mechanics and Mining Sciences*, vol. 50, pp. 170–173, 2012.

[24] K. Han, J. W. W. Ju, H. Kong, and M. Wang, "Functional catastrophe analysis of progressive failures for deep tunnel roof considering variable dilatancy angle and detaching velocity," *Rock Mechanics and Rock Engineering*, vol. 52, no. 10, pp. 3987–3997, 2019.

[25] C. B. Qin, S. C. Chian, and X. L. Yang, "3D limit analysis of progressive collapse in partly weathered Hoek–Brown rock banks," *International Journal of Geomechanics*, vol. 17, no. 7, Article ID 04017011, 2017.

[26] C. B. Qin, X. L. Yang, Q. J. Pan, Z. B. Sun, L. L. Wang, and T. Miao, "Upper bound analysis of progressive failure mechanism of tunnel roofs in partly weathered stratified Hoek-Brown rock masses," *International Journal of Rock Mechanics and Mining Sciences*, vol. 74, pp. 157–162, 2015.

[27] Y. Gao, Z. Yang, Z. Cheng, Y. Jiang, and Y. Ren, "Limit analysis of tunnel collapse according to the Hoek-Brown criterion and bolt parameter research," *Arabian Journal for Science and Engineering*, vol. 44, no. 10, pp. 8171–8180, 2019.

[28] K. Guan, W. C. Zhu, L. L. Niu, and Q. Y. Wang, "Three-dimensional upper bound limit analysis of supported cavity roof with arbitrary profile in Hoek-Brown rock mass," *Tunnelling and Underground Space Technology*, vol. 69, no. June, pp. 147–154, 2017.

[29] B. Jiang, Q. Wang, S. C. Li et al., "The research of design method for anchor cables applied to cavern roof in water-rich strata based on upper-bound theory," *Tunnelling and Underground Space Technology*, vol. 53, pp. 120–127, 2016.

[30] F. Yang and X. L. Yang, "Upper bound limit analysis of collapse shape for circular tunnel subjected to pore pressure based on the Hoek-Brown failure criterion," *Tunnelling and Underground Space Technology*, vol. 26, no. 5, pp. 614–618, 2011.

[31] C. Qin, S. C. Chian, X. Yang, and D. Du, "2D and 3D limit analysis of progressive collapse mechanism for deep-buried tunnels under the condition of varying water table," *International Journal of Rock Mechanics and Mining Sciences*, vol. 80, pp. 255–264, 2015.

[32] L. Yu, C. Lyu, M. Wang, and T. Xu, "Three-dimensional upper bound limit analysis of a deep soil-tunnel subjected to pore pressure based on the nonlinear Mohr-Coulomb criterion," *Computers and Geotechnics*, vol. 112, no. April, pp. 293–301, 2019.

[33] R. Zhang and X. Yang, "Limit analysis of active and passive mechanisms of shallow tunnels in nonassociative soil with changing water table," *International Journal of Geomechanics*, vol. 18, no. 7, Article ID 04018063, 2018.

[34] S. W. Jacobsz, "Trapdoor experiments studying cavity propagation," *Proceedings of the First Southern African Geotechnical Conference*, in *Proceedings of the 1st Southern African Geotechnical Conference*, pp. 159–165, 2016. November.

[35] F. Huang, H. Zhu, Q. Xu, Y. Cai, and X. Zhuang, "The effect of weak interlayer on the failure pattern of rock mass around tunnel - scaled model tests and numerical analysis," *Tunnelling and Underground Space Technology*, vol. 35, pp. 207–218, 2013.

[36] D. P. Xu, X. T. Feng, Y. J. Cui, and Q. Jiang, "Use of the equivalent continuum approach to model the behavior of a rock mass containing an interlayer shear weakness zone in an underground cavern excavation," *Tunnelling and Underground Space Technology*, vol. 47, pp. 35–51, 2015.

[37] Y. Zhao, Q. Gong, Y. Wu, Z. Tian, S. Zhou, and L. Fu, "Progressive failure mechanism in granular materials subjected to an alternant active and passive trapdoor," *Transportation Geotechnics*, vol. 28, Article ID 100529, 2021.

[38] C. p. Zhang, K. h. Han, Q. Fang, and D. l. Zhang, "Functional catastrophe analysis of collapse mechanisms for deep tunnels based on the Hoek-Brown failure criterion," *Journal of Zhejiang University - Science*, vol. 15, no. 9, pp. 723–731, 2014.

[39] R. M. Caddell, R. S. Raghava, and A. G. Atkins, "A yield criterion for anisotropic and pressure dependent solids such as oriented polymers," *Journal of Materials Science*, vol. 8, no. 11, pp. 1641–1646, 1973.

[40] H. J. Greenberg, *On the Variational Principles of Mechanics*, 1949.

[41] W.-F. Chen, *Limit Analysis and Soil Plasticity*, 1975.

[42] T. Yang and X. Yang, "Limit analysis of failure mechanism of tunnel roof collapse considering variable detaching velocity along yield surface," *International Journal of Rock Mechanics and Mining Sciences*, vol. 100, no. October, pp. 229–237, 2017.